Volume-optimal persistence homological scaffolds of hemodynamic networks covary with MEG theta-alpha aperiodic dynamics

Nghi Nguyen[1], Tao Hou[2], Enrico Amico[3], Jingyi Zheng[4], Huajun Huang[4], Alan D. Kaplan[5], Giovanni Petri[6], Joaquín Goñi[7,8], Ralph Kaufmann[9], Yize Zhao[10], Duy Duong-Tran[11,12,13,†], and Li Shen[12,13]

[1] Multidisciplinary Brain Research Center, Bar-Ilan University, Ramat Gan, Israel
[2] Department of Computer Science, University of Oregon, Eugene, Oregon, USA
[3] Institute of Health and Neurodevelopment, College of Health and Life Sciences, Aston University, Birmingham, UK
[4] Department of Mathematics and Statistics, Auburn University, Alabama, USA
[5] Computational Engineering Division, Lawrence Livermore National Laboratory, Livermore, California, USA
[6] NPLab, Network Science Institute, Northeastern University London, London, UK
[7] School of Industrial Engineering, Purdue University, West Lafayette, Indiana, USA
[8] School of Biomedical Engineering, Purdue University, W. Lafayette, Indiana, USA
[9] Department of Mathematics, Purdue University, West Lafayette, IN, USA
[10] School of Public Health, Yale University, New Heaven, Connecticut, USA
[11] Department of Mathematics, U.S. Naval Academy, Annapolis, Maryland, USA
[12] Department of Biostatistics, Epidemiology and Informatics, University of Pennsylvania, Philadelphia, Pennsylvania, USA{duyanh.duong-tran,li.shen}@pennmedicine.upenn.edu
[13] Co-supervising authors
† Corresponding author

Abstract. Higher-order properties of functional magnetic resonance imaging (fMRI) induced connectivity have been shown to unravel many exclusive topological and dynamical insights beyond pairwise interactions. Nonetheless, whether these fMRI-induced higher-order properties play a role in disentangling other neuroimaging modalities' insights remains largely unexplored and poorly understood. In this work, by analyzing fMRI data from the Human Connectome Project Young Adult dataset using persistent homology, we discovered that the volume-optimal persistence homological scaffolds of fMRI-based functional connectomes exhibited conservative topological reconfigurations from the resting state to attentional task-positive state. Specifically, while reflecting the extent to which each cortical region contributed to functional cycles following different cognitive demands, these reconfigurations were constrained such that the spatial distribution of cavities in the connectome is relatively conserved. Most importantly, such level of contributions covaried with powers of aperiodic activities mostly within the theta-alpha (4-12 Hz) band measured by magnetoencephalography (MEG). This comprehensive result suggests that fMRI-induced hemodynamics and MEG theta-alpha aperiodic activities are governed by the same functional constraints

specific to each cortical morpho-structure. Methodologically, our work paves the way toward an innovative computing paradigm in multimodal neuroimaging topological learning. The code for our analyses is provided in `https://github.com/ngcaonghi/scaffold_noise`.

1   Introduction

Many real-world systems can be characterized not only by graphs, which are described by nodes and pairwise relations but also by complexes and hypergraphs, elucidating higher-order relations [14,13]. Interactions between these higher-order structures have been demonstrated to elucidate complex dynamics, such as phase transitions induced by emergent phenomena in complex networks [4], that could not be fully explained by pairwise interactions alone. In neuroscience, brain dynamics analysis based on such higher-order descriptions of neuronal populations has yielded statistically and topologically significant results [14,27,10,9]. Underlying such successes is a family of analytical tools commonly referred to as Topological Data Analysis (TDA) [8,11], which includes persistent homology (PH) [11]. Using PH on functional connections deriving from functional magnetic resonance imaging (fMRI), several studies have identified differences between cognitive abilities [24], brain states [24], and brain regions [21,9] in terms of higher-order features (e.g., topological invariants) pertaining to voids (cavities) and cycles. However, the relationships between these topological invariants (e.g., cycles) and other neural correlates, such as anatomical structures and electrophysiological dynamics, remain poorly understood.

Among such neural correlates are cortical aperiodic dynamics, which have recently gained growing interest due to their implicated roles in cognition [23], consciousness [28], aging [31], and diseases [25,26]. Generative mechanisms of these dynamics, particularly those within the gamma band (> 30 Hz), have been linked to several biological processes [19]. However, aperiodic activities on the level of cortical regions below the gamma band (< 30 Hz) are significantly less understood.

In this study, using the notion of PH *scaffolds* developed by Petri *et al.* [24], we associate a critical link between fMRI-induced human brain large-scale functional connectivity cycles and aperiodic magnetoencephalography (MEG) activities in theta-alpha range (4-12 Hz). Specifically, we discovered that for each parcellated region in the cortex, changes in its contribution to maintaining homological cycle persistence were positively correlated with changes in its theta-alpha aperiodic power. Comprehensively, our pioneering work paves the way toward a new, innovative computing paradigm in multimodal neuroimaging topological learning.

2   Methods

2.1   Overview of Topological Data Analysis

Topological Data Analysis (TDA) [8] is an emerging field focusing on understanding the "shape" of data (denoted as X) through homology theory [7]. Classical homology groups [7] capture voids and cycles of topological spaces in various dimensions i (e.g., connected components ($i = 0$), rings ($i = 1$), and cavities ($i = 2$), and so on). Functional connectomes (FCs, denoted as G) in this paper refer to symmetric matrices, whose entries are pair-wise functional couplings quantified by Pearson correlations, realized from X. Extracting topological information involves mapping an FC onto a topological space by constructing its simplicial clique complex $\Delta(G)$, which represents higher-order interactions: $G \to \Delta(G)$. This involves defining a threshold r sampled from a set of distinct weight values in FC, which determines a corresponding binarized scaffold $G(r)$. The associated homology groups $H_i(\Delta(G))$ then become a function of r. Along the process of scanning r from 0 to 1, homology is born and annihilated. The sequence of these births and deaths is mathematically captured by *persistence homology* [11].

More precisely speaking, the simplicial clique complex $\Delta(G)$ takes the form of a *filtration* $\mathcal{F} : K_0 \subseteq K_1 \subseteq \cdots \subseteq K_m$, which is a growing sequence of discretized spaces yielded along the scanning process from 0 to 1. In $\mathcal{F}$, each simplicial complex K_i is a union of building blocks such as vertices, edges, triangles, and higher dimensional analogs. Given a filtration $\mathcal{F}$, persistent homology produces a set of intervals—called the *barcode*—as a scheme for quantifying the "significance" (e.g. persistence) of topological features in spaces. In the barcode of $\mathcal{F}$, each interval registers the birth and death of a homology feature in the sequence with the longer intervals typically considered to correspond to more significant features (see [6,8]).

2.2   Volume-optimal Persistent Cycles

Although *cycles* make up features in homology, the barcode of a filtration $\mathcal{F}$ does not provide concrete representative cycles for the homology features born and died in the sequence. However, these representatives for persistent homology, termed as *persistent cycles*, reveal rather crucial insights into the topological spaces over which filtrations are taken.

Definition 1. *For an interval $[b, d)$ in the barcode of $\mathcal{F}$, a* persistent cycle *for $[b, d)$ is a cycle born in K_b (existing in K_b but not in K_{b-1}) and becoming trivial in K_d (is not a boundary in K_{d-1} but becomes a boundary in K_d).*

As indicated in several works (e.g., [22]), an interval in the barcode could have more than one persistent cycle, among which a canonical choice is to compute an *optimized* persistent cycle with weights typically reflecting the intrinsic areas of the cycles. Such weight-optimized cycles can provide the tightest representations of the holes characterized by persistent homology. However, Dey et al. [7] showed

that computing optimal persistent cycles is NP-hard in general. In this paper, we utilize a Python library called `HomCloud` developed by Obayashi [22] for computing persistent cycles. `HomCloud` uses a linear-program-based algorithm for computing optimized persistent cycles and indeed targets *volume-optimal* persistent cycles, where weights of the higher dimensional bounding chains are optimized. In this paper, we found that the persistent cycles produced by `HomCloud` typically have good quality (better than the non-optimized ones produced by the original persistence algorithm [11]). More importantly, mathematical constructs based on such cycles can afford additional interpretations about the volume of the cavities that they wrap around.

2.3   HCP data processing

Persistence homological scaffolds of resting-state and task-based hemodynamic networks. We used resting-state and task-based 3T fMRI data from a subset of the Human Connectome Project Young Adult dataset [29], preprocessed by the Neuromatch Academy [16]. Our study focused on left-hand, right-hand, left-foot, and right-foot motor tasks, and 0-back faces, 0-back tools, 2-back faces, and 2-back tools working memory tasks. To ensure valid extrapolation to MEG neural correlates, we excluded 20 subjects that underwent the same task conditions during MEG recording trials. The resulting sample size was N = 319, each of which represents the BOLD signals of one subject under resting and task conditions and parcellated according to the Glasser atlas [15].

Functional connectivity matrices were computed for each subject by computing Pearson correlation coefficients between BOLD time series of region pairs. To perform persistent cycle discovery with `HomCloud` on every connectivity matrix G, we converted each pairwise correlation term r into a pseudo-distance index $\omega := 1 - r$ while excluding negative correlations (figure 1.I.A). For each pseudo-distance matrix with weights $\{\omega\}$, we generated a Vietoris-Rips filtration $\mathcal{F}$ of the homological group H_1. Every complex in $\mathcal{F}$ entailed a birth-death interval $[b, d)$ where $b, d \in \{\omega\}$, a volume-optimal persistent cycle g_t, and its persistence $\pi_{g_t} = d - b$ (figures 1.I.B and 1.I.C). From this point, we followed the approach outlined by Petri *et al.* [24] to calculate the *persistence homological scaffold network* $\mathcal{H}_G^p$ composed of the volume-optimal cycles (figure 1.I.D). Specifically, for every edge $e_{i,j}$ between nodes i and j belonging to multiple cycles $g_0, g_1, \cdots, g_s$, its weight is $w_{i,j}^\pi = \sum_{g_t | e_{i,j} \in g_t} \pi_{g_t}$. The group-averaged scaffold matrix was generated for each experimental condition (figure 1.I.E), from which we calculated the *persistence centrality* (PC) indices defined by $PC(i) = \sum_j w_{i,j}^\pi \left(\sum_{j,k} w_{j,k}^\pi \right)^{-1}$ for each node i (figure 1.I.F). For comparative purposes, we also calculated the degree centrality (DC) indices from the original functional connectivity matrix G with edge weights $\{r\}$, whereby $DC(i) = (\sum_j r_{i,j})(\sum_{j,k} r_{j,k})^{-1}$.

MEG data preprocessing. We used MEG data from the same HCP dataset under the same task conditions but with the subjects previously excluded from
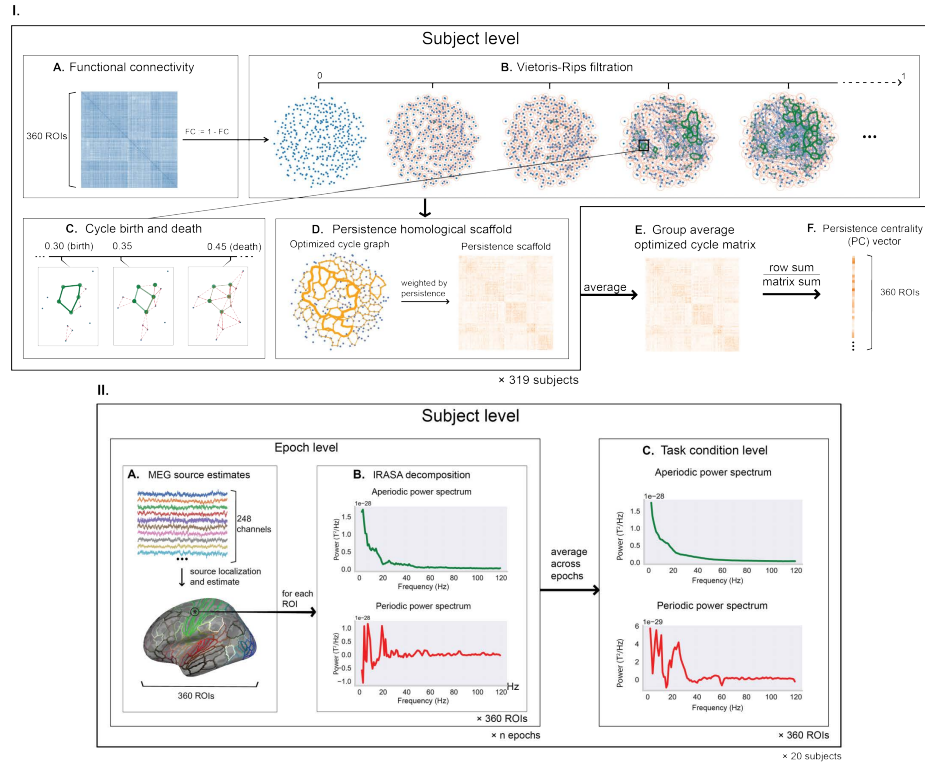
Fig. 1. Data processing pipelines. I. From fMRI functional connectivity to persistence centrality. II. From sensor-level MEG signals to Glasser-parcellated power spectrum decomposition.

the fMRI data analysis (n = 20) and preprocessed as previously detailed by Larson-Prior et al., 2013 [20]. Each subject's data comprised 12-second segments of randomly epoched resting-state data and task-evoked data starting from the first stimulus onset of each task block. We performed source reconstruction using linearly constrained minimum variance (LCMV) beamformers [30] on boundary element method (BEM) surfaces derived from subject anatomy data. The source estimates were then grouped by labels defined by the Glasser atlas and averaged across sources (figure 1.II.A), resulting in a single time series per epoch for every Glasser region.

Power spectrum decomposition. On each Glasser-parcellated MEG epoch, we computed the power spectral density using Welch's method (with 2-second Hann windows and 1-second overlaps) and performed spectrum decomposition using the irregular-resampling auto-spectral analysis (IRASA) method developed by Wen & Liu, 2015 [32]. The resulting aperiodic and periodic spectra spanned a

frequency band of 1 to 120 Hz (Figure 1.II.B). Epoch-level spectra were averaged to produce those for the resting state and every task condition (Figure 1.II.C). To avoid high-frequency artifacts that might contaminate downstream analyses, we only considered power in the range of 1 to 90 Hz.

3   Result

3.1   Directions of change in persistence centralities are consistent across attentional task conditions
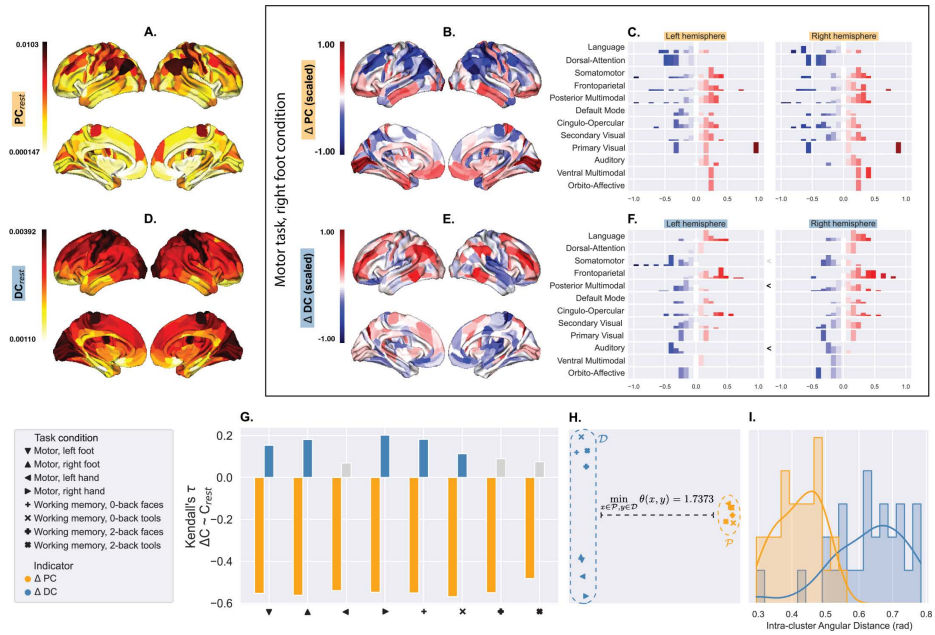
Fig. 2. Resting state-subtracted PC (ΔPC) captures task-evoked hemodynamic patterns nonspecific to task conditions, whereas resting state-subtracted DC (ΔDC) is more condition-specific.

In Figure 2.A and 2.D, the spatial distributions of resting-state PC and DC are portrayed on a Glasser-parcellated surface. Figure 2.B maps ΔPC, representing the PCs during the motor task and right foot condition subtracted by the resting-state PCs, on the same brain surface. The mapped surface shows a coarse-grained global gradient of ΔPC starting from the deepest ΔPC sinks (in blue) in the dorsal areas to the sources (in red) in ventral regions. Notably, this gradient does not exhibit a hemisphere asymmetry (figure 2.C), as evidenced by similar distributions of sinks and sources across hemispheres for each functional

network ($p > 0.34 > 0.05$, Mann-Whitney U-test). Figures 2.E and 2.F demonstrate the ΔDC counterparts of figures 2.B and 2.C, respectively, revealing a different distribution of sinks and sources that shows hemispheric asymmetry. See Supplementary information, figures S1 and S2 for a comprehensive comparison of PC, DC, ΔPC, and ΔDC distributions across all task conditions.

Figure 2.G demonstrates the relationship between resting-state PC (or DC) and ΔPC (or ΔDC) evoked by each task condition. All ΔPC vectors have strongly negative correlations with the resting-state PC ($p << 0.05$, Kendall's τ for rank association), while their ΔDC counterparts show weak or non-significant correlations. ΔPC and ΔDC clusters are at least not positively correlated as demonstrated by the minimum angular difference of 1.7373 radians, $i.e.$, nearly orthogonal (visualized by multidimensional scaling, MDS, in figure 2.H). Figure 2.I sketches the distributions of angular differences within each cluster, showing that spatial patterns of PC sinks and sources are more consistent across tasks and conditions than those of DC.

From the observations above, we concluded that ΔPC was more correlated with changes in cognitive demand than with the nature of the task, while ΔDC was task-specific. Spatially, ΔPC exhibited patterns such as "sinks" concentrated in the Dorsal-Attention network and "sources" in the Auditory network and part of the Cingulo-Opercular network previously identified as the salience network [18]. Such "sink" and "source" regions indicated the reduction and increase, respectively, of the volumes of functional connectome cavities incident to those regions. Since the spatial distributions of ΔPC "sinks" and "sources" were consistent across task conditions (Supplementary information, figures S1), we further concluded that under different cognitive demands, cavities in the functional connectomes were conserved in space and relatively invariant to changes in cortical computations.

3.2 Persistence centralities and theta-alpha aperiodic band powers change in the same direction

We observed that ΔPC coincided with aperiodic dynamic patterns outlined in previous fMRI-EEG studies [17]. Further corroborating this correlation, cosine similarities between ΔPC and changes in band power ratios ($\Delta BPRs$) within the theta-alpha range were significantly higher than those between $\Delta BPRs$ and ΔDC.

Figures 3.A and 3.B present Isomap projections of ΔPC and ΔDC, respectively, evoked by right-foot cues during the motor task. These allow for visual comparison with the Δ BPR of canonical bands (delta: 2-4 Hz, theta: 4-8 Hz, alpha: 8-12 Hz, beta: 12-25 Hz, gamma: 25-90 Hz), also projected using Isomap and depicted in figures 3.C to 3.G. Δ BPR was also computed for 32 frequency bands whose endpoints were logarithmically spaced within the range of 2 to 90 Hz. Cosine similarities between these Δ BPRs and ΔPC (orange) or ΔDC (blue) under the motor, right-foot condition are shown in Figure 3.H. Absolute cosine similarities averaged across conditions are shown in Figure 3.I, suggesting that ΔPC better predicts Δ BPRs in the theta-alpha and gamma ranges (p =
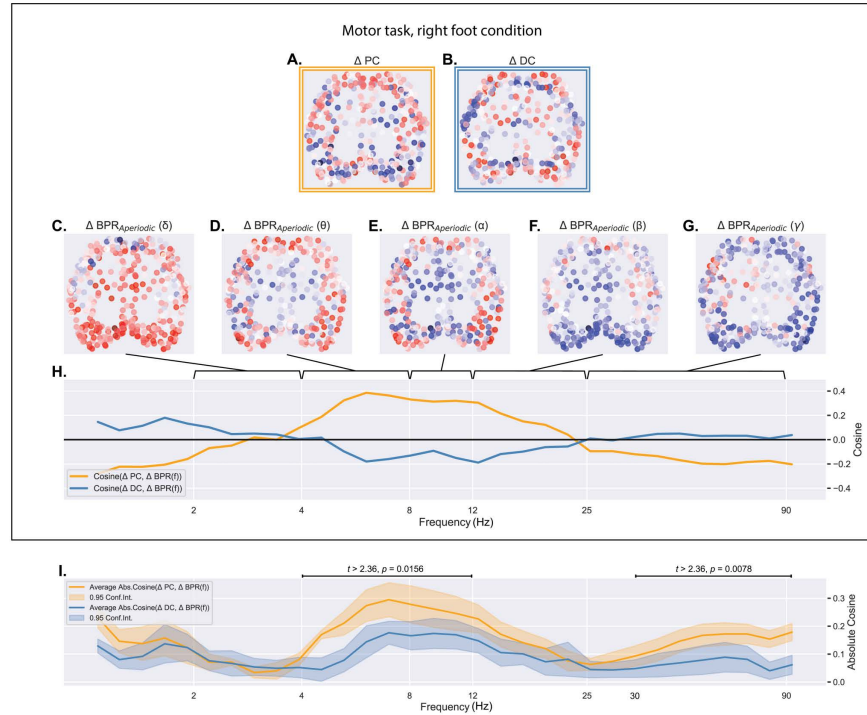
Fig. 3. Regional alterations in bandpower ratio (Δ BPR) of cortical aperiodic activity within the theta-alpha range (4 - 12 Hz) exhibit a stronger alignment with ΔPC compared to ΔDC.

0.0156 and p = 0.0078, respectively, cluster-based permutation paired t-test). Similar analyses for the periodic component resulted in statistically insignificant correlations between periodic activities and ΔPC or ΔDC.

4   Discussion

By exploring the relationship between fMRI and MEG data from a novel bi-modal perspective, this study reveals two previously undocumented phenomena. Firstly, the persistence centrality (PC) of each cortical structure, representing its participation in persistent cycles relative to the total participation, demonstrates predictable changes between brain states induced by different attentional demands. Specifically, regardless of the task nature, functional cavities incident to structures with high PCs tend to contract when attention is required, and vice versa. Secondly, the directions of change in PC predict those in the power of theta-alpha aperiodic activities on the brain-wide scale. These observations underscore a relationship between BOLD signals and electrophysiological activ-

ities that pairwise interactions, if represented only by node degrees, cannot fully describe. In other words, it must rely on the notion of volume-optimal functional cycles.

Since changes in these functional cycles and their associated changes in the aperiodic spectra are robust across normal brain states, it might be possible that they emerge from a common constraint regime governing both hemodynamics and aperiodic electrodynamics that vary among subjects (e.g., fingerprint [1,2,5,3,12]). This relatively new notion of a constraint regime described by cycles suggests new directions toward understanding the generative mechanisms of BOLD signals and sub-gamma aperiodic spectra. Future investigations—which might involve connections to subcortical structures such as the thalamus—can help detail or expand the current models of BOLD functional connectivity on the systemic macrovascular level. More broadly, by leveraging topological assumptions that persist throughout different normal brain states, homological cycles in the brain can provide better guidance for treatments of outlying brain states indicative of psychological disorders, neuropathologies, and neurodegeneration.

Disclosure of Interests. The authors have no competing interests to declare that are relevant to the content of this article.

References

1. Abbas, K., Amico, E., Svaldi, D.O., Tipnis, U., Duong-Tran, D.A., Liu, M., Rajapandian, M., Harezlak, J., Ances, B.M., Goñi, J.: Geff: Graph embedding for functional fingerprinting. NeuroImage **221**, 117181 (2020)
2. Abbas, K., Liu, M., Wang, M., Duong-Tran, D., Tipnis, U., Amico, E., Kaplan, A.D., Dzemidzic, M., Kareken, D., Ances, B.M., et al.: Tangent functional connectomes uncover more unique phenotypic traits. Iscience **26**(9) (2023)
3. Amico, E., Abbas, K., Duong-Tran, D.A., Tipnis, U., Rajapandian, M., Chumin, E., Ventresca, M., Harezlak, J., Goñi, J.: Toward an information theoretical description of communication in brain networks. Network Neuroscience **5**(3), 646–665 (2021)
4. Battiston, F., Amico, E., Barrat, A., Bianconi, G., Ferraz de Arruda, G., Franceschiello, B., Iacopini, I., Kéfi, S., Latora, V., Moreno, Y., et al.: The physics of higher-order interactions in complex systems. Nature Physics **17**(10), 1093–1098 (2021)
5. Chiêm, B., Abbas, K., Amico, E., Duong-Tran, D.A., Crevecoeur, F., Goñi, J.: Improving functional connectome fingerprinting with degree-normalization. Brain Connectivity **12**(2), 180–192 (2022)

6. Cohen-Steiner, D., Edelsbrunner, H., Harer, J.: Stability of persistence diagrams. Discrete & Computational Geometry **37**(1), 103–120 (2007)

7. Dey, T.K., Hou, T., Mandal, S.: Computing minimal persistent cycles: Polynomial and hard cases. In: Proceedings of the Fourteenth Annual ACM-SIAM Symposium on Discrete Algorithms. pp. 2587–2606. SIAM (2020)

8. Dey, T.K., Wang, Y.: Computational Topology for Data Analysis. Cambridge University Press (2022)

9. Duong-Tran, D., Kaufmann, R., Chen, J., Wang, X., Garai, S., Xu, F.H., Bao, J., Amico, E., Kaplan, A.D., Petri, G., et al.: Homological landscape of human brain functional sub-circuits. Mathematics **12**(3), 455 (2024)

10. Duong-Tran, D., Kausar, A., Amico, E., Corominas-Murtra, B., Dzemidzic, M., Kareken, D., Ventresca, M., Goñi, J.: A morphospace of functional configuration to assess configural breadth based on brain functional networks. Network Neuroscience pp. 1–36 (2021)

11. Edelsbrunner, H., Harer, J.: Computational topology: an introduction. American Mathematical Soc. (2010)

12. Garai, S., Xu, F., Duong-Tran, D.A., Zhao, Y., Shen, L.: Mining correlation between fluid intelligence and whole-brain large scale structural connectivity. AMIA Summits on Translational Science Proceedings **2023**, 225 (2023)

13. Giusti, C., Ghrist, R., Bassett, D.S.: Two's company, three (or more) is a simplex. Journal of computational neuroscience **41**(1), 1–14 (2016)

14. Giusti, C., Pastalkova, E., Curto, C., Itskov, V.: Clique topology reveals intrinsic geometric structure in neural correlations. Proceedings of the National Academy of Sciences **112**(44), 13455–13460 (2015)

15. Glasser, M.F., Coalson, T.S., Robinson, E.C., Hacker, C.D., Harwell, J., Yacoub, E., Ugurbil, K., Andersson, J., Beckmann, C.F., Jenkinson, M., et al.: A multimodal parcellation of human cerebral cortex. Nature **536**(7615), 171–178 (2016)

16. t Hart, B., Achakulvisut, T., Adeyemi, A., Akrami, A., Alicea, B., Alonso-Andres, A., Alzate-Correa, D., Ash, A., Ballesteros, J., Balwani, A., et al.: Neuromatch academy: a 3-week, online summer school in computational neuroscience. Journal of Open Source Education **5**(49), 118 (2022)

17. Jacob, M.S., Roach, B.J., Sargent, K.S., Mathalon, D.H., Ford, J.M.: Aperiodic measures of neural excitability are associated with anticorrelated hemodynamic networks at rest: a combined eeg-fmri study. NeuroImage **245**, 118705 (2021)

18. Ji, J.L., Spronk, M., Kulkarni, K., Repovš, G., Anticevic, A., Cole, M.W.: Mapping the human brain's cortical-subcortical functional network organization. Neuroimage **185**, 35–57 (2019)

19. Kramer, M.A., Chu, C.J.: The 1/f-like behavior of neural field spectra are a natural consequence of noise driven brain dynamics. bioRxiv pp. 2023–03 (2023)

20. Larson-Prior, L.J., Oostenveld, R., Della Penna, S., Michalareas, G., Prior, F., Babajani-Feremi, A., Schoffelen, J.M., Marzetti, L., de Pasquale, F., Di Pompeo, F., et al.: Adding dynamics to the human connectome project with meg. Neuroimage **80**, 190–201 (2013)

21. Lord, L.D., Expert, P., Fernandes, H.M., Petri, G., Van Hartevelt, T.J., Vaccarino, F., Deco, G., Turkheimer, F., Kringelbach, M.L.: Insights into brain architectures from the homological scaffolds of functional connectivity networks. Frontiers in systems neuroscience **10**, 85 (2016)

22. Obayashi, I.: Volume-optimal cycle: Tightest representative cycle of a generator in persistent homology. SIAM Journal on Applied Algebra and Geometry **2**(4), 508–534 (2018)

23. Ouyang, G., Hildebrandt, A., Schmitz, F., Herrmann, C.S.: Decomposing alpha and 1/f brain activities reveals their differential associations with cognitive processing speed. NeuroImage **205**, 116304 (2020)
24. Petri, G., Expert, P., Turkheimer, F., Carhart-Harris, R., Nutt, D., Hellyer, P.J., Vaccarino, F.: Homological scaffolds of brain functional networks. Journal of The Royal Society Interface **11**(101), 20140873 (2014)
25. Robertson, M.M., Furlong, S., Voytek, B., Donoghue, T., Boettiger, C.A., Sheridan, M.A.: Eeg power spectral slope differs by adhd status and stimulant medication exposure in early childhood. Journal of Neurophysiology **122**(6), 2427–2437 (2019)
26. Rosenblum, Y., Shiner, T., Bregman, N., Giladi, N., Maidan, I., Fahoum, F., Mirelman, A.: Decreased aperiodic neural activity in parkinson's disease and dementia with lewy bodies. Journal of Neurology pp. 1–12 (2023)
27. Schneidman, E., Berry, M.J., Segev, R., Bialek, W.: Weak pairwise correlations imply strongly correlated network states in a neural population. Nature **440**(7087), 1007–1012 (2006)
28. Toker, D., Pappas, I., Lendner, J.D., Frohlich, J., Mateos, D.M., Muthukumaraswamy, S., Carhart-Harris, R., Paff, M., Vespa, P.M., Monti, M.M., et al.: Consciousness is supported by near-critical slow cortical electrodynamics. Proceedings of the National Academy of Sciences **119**(7), e2024455119 (2022)
29. Van Essen, D.C., Smith, S.M., Barch, D.M., Behrens, T.E., Yacoub, E., Ugurbil, K., Consortium, W.M.H., et al.: The wu-minn human connectome project: an overview. Neuroimage **80**, 62–79 (2013)
30. Van Veen, B.D., Van Drongelen, W., Yuchtman, M., Suzuki, A.: Localization of brain electrical activity via linearly constrained minimum variance spatial filtering. IEEE Transactions on biomedical engineering **44**(9), 867–880 (1997)
31. Voytek, B., Kramer, M.A., Case, J., Lepage, K.Q., Tempesta, Z.R., Knight, R.T., Gazzaley, A.: Age-related changes in 1/f neural electrophysiological noise. Journal of Neuroscience **35**(38), 13257–13265 (2015)
32. Wen, H., Liu, Z.: Separating fractal and oscillatory components in the power spectrum of neurophysiological signal. Brain topography **29**, 13–26 (2016)